Contributions of inflammation and tumor microenvironment to neurofibroma tumorigenesis

Chung-Ping Liao,[1] Reid C. Booker,[1] Jean-Philippe Brosseau,[1] Zhiguo Chen,[1] Juan Mo,[1] Edem Tchegnon,[1] Yong Wang,[1] D. Wade Clapp,[2] and Lu Q. Le[1,3,4,5]

[1]Department of Dermatology, University of Texas Southwestern Medical Center, Dallas, Texas, USA. [2]Department of Pediatrics, Indiana University School of Medicine, Indianapolis, Indiana, USA. [3]Neurofibromatosis Clinic, [4]Simmons Comprehensive Cancer Center, and [5]Hamon Center for Regenerative Science and Medicine, University of Texas Southwestern Medical Center, Dallas, Texas, USA.

Neurofibromatosis type 1 associates with multiple neoplasms, and the Schwann cell tumor neurofibroma is the most prevalent. A hallmark feature of neurofibroma is mast cell infiltration, which is recruited by chemoattractant stem cell factor (SCF) and has been suggested to sustain neurofibroma tumorigenesis. In the present study, we use new, genetically engineered *Scf* mice to decipher the contributions of tumor-derived SCF and mast cells to neurofibroma development. We demonstrate that mast cell infiltration is dependent on SCF from tumor Schwann cells. However, removal of mast cells by depleting the main SCF source only slightly affects neurofibroma progression. Other inflammation signatures show that all neurofibromas are associated with high levels of macrophages regardless of *Scf* status. These findings suggest an active inflammation in neurofibromas and partly explain why mast cell removal alone is not sufficient to relieve tumor burden in this experimental neurofibroma model. Furthermore, we show that plexiform neurofibromas are highly associated with injury-prone spinal nerves that are close to flexible vertebras. In summary, our study details the role of inflammation in neurofibromagenesis. Our data indicate that prevention of inflammation and possibly also nerve injury at the observed tumor locations are therapeutic approaches for neurofibroma prophylaxis and that such treatment should be explored.

Introduction

Neurofibromatosis type 1 (NF1, formerly known as von Recklinghausen disease) is an autosomal dominant genetic disorder. The prevalence of NF1 is approximately 1 in 3,500 births, regardless of sex and race (1–3). The common clinical presentations of NF1 include neurofibromas, café-au-lait macules on the skin, freckles under the armpits or in the groin areas, Lisch nodules in the eyes, optic gliomas, scoliosis, and bone enlargement or malformation. Homozygous loss of *NF1* caused by *NF1* loss of heterozygosity can give rise to multiple types of neoplasms, and neurofibroma is the most common among them (2–7).

Neurofibroma is a nerve sheath tumor developing in the peripheral nervous system that can present in different distinct forms. However, for simplicity, most clinicians divide neurofibromas into (a) cutaneous neurofibromas, which grow along cutaneous nerve twigs as numerous tumor nodules on the skin, and (b) plexiform neurofibromas, which develop along an internal nerve plexus. Plexiform neurofibromas continue to grow throughout life and there is a 10% lifetime risk for them to transform into malignant peripheral nerve sheath tumors (8), life-threatening malignancies. Current clinical treatment options for neurofibromas are limited to surgical resection, although pharmacological inhibition of MEK has recently shown success in an experimental animal model (9) and in the early phase of a clinical trial (10).

Neurofibromas are heterogeneous tumors comprised of neoplastic Schwann cells and nonneoplastic fibroblasts, vascular endothelial cells, and mast cells, as well as dense collagen. The presence of mast cell infiltration can be frequently observed in neurofibromas (11–14); however, it is not common in other types of neoplasms. The neurofibroma-associated mast cells appear to be at activated status, as levels of local histamine content (13) and circulating serum IgE are high (15). This unique characteristic feature has made mast cells a target of interest in neurofibroma research. Efforts have been made to understand the role of mast cells in the neurofibroma tumor microenvironment, and most importantly, to determine whether mast cell metabolism could be a viable therapeutic target against neurofibromas (6, 16, 17).

Mast cells are immune effector cells that feature a high content of secretory granules containing multiple types of immunomodulatory molecules, such as histamine. Therefore, therapeutic approaches have attempted to prevent the growth of neurofibromas by stabilizing mast cell activity. Riccardi reported the use of antihistamine agent ketotifen (histamine H1-receptor antagonist) to hamper the growth of neurofibroma (18) and to reduce tumor-associated pain and itching (19). Recently, Riccardi reported that a patient with NF1 received beneficial responses from long-term ketotifen treatment by showing far fewer cutaneous neurofibromas compared with an age-matched control (20). These clinical findings further suggested that mast cells could play a supportive role in neurofibroma development and mast cell metabolism might be a druggable target.

Distinct from other differentiated blood cell types, mast cells express the KIT receptor, which is activated by stem cell factor

Conflict of interest: The authors have declared that no conflict of interest exists.
Submitted: December 26, 2017; **Accepted:** March 27, 2018.
Reference information: *J Clin Invest*. 2018;128(7):2848–2861.
https://doi.org/10.1172/JCI99424.

(SCF). SCF/KIT signaling drives cell proliferation, migration, and survival in selected cell types (21). The action of SCF/KIT signaling has been recognized in the following cellular interactions: (a) hematopoietic stem cells (KIT) and endothelial/perivascular cells (SCF) (22) (b) melanocyte (KIT) and epithelial keratinocytes (SCF) (23), and (c) germ cells (KIT) and surrounding somatic cells (SCF) (24). In local tissues, SCF is also a strong chemoattractant to induce mast cell chemotaxis from circulating blood into local tissues (25). Furthermore, SCF can activate mast cell degranulation to release immunomodulatory molecules (26, 27). Therefore, identification of the SCF-expressing cells within the tumor microenvironment is critical to delineate the mast cell infiltration in neurofibroma. A set of in vitro experiments using culture cells has shown that Schwann cells express SCF and that their SCF can induce mast cell migration (28). Interestingly, mast cell migration ability is associated with the *Nf1* status in both Schwann cells and mast cells; the strongest combination is $Nf1^{-/-}$ Schwann cells with $Nf1^{+/-}$ mast cells (28). This synergistic effect was achieved by the high SCF expression in $Nf1^{-/-}$ Schwann cells (28) and the *Nf1* haploinsufficiency in mast cells (29, 30).

In addition to SCF signaling, *Nf1* heterozygosity has also been considered a critical factor in neurofibroma development. The importance of *Nf1* heterozygosity was first noticed in the pioneer mouse plexiform neurofibroma model in which the $Nf1^{f/-}$ *Krox20-Cre* mice developed tumors but the $Nf1^{f/f}$ *Krox20-Cre* mice (31) did not, highlighting the contribution of $Nf1^{+/-}$ to the tumor microenvironment. Yang and colleagues further delineated the critical role of $Nf1^{+/-}$ nontumor cells from hematopoietic cells by bone marrow transplantation experiments (16) and implied $Nf1^{+/-}$ mast cells as critical contributors to sustain the neurofibroma microenvironment. Nevertheless, *Nf1* heterozygosity does not seem to be always required in all neurofibroma mouse models. For example, $Nf1^{f/f}$ *Dhh-Cre* mice developed plexiform neurofibroma without an $Nf1^{+/-}$ microenvironment (32). In this study, by employing new genetic mouse models, we comprehensively evaluate the contributions of SCF and *Nf1* heterozygosity in the neurofibroma tumor microenvironment to better understand the roles of these factors in neurofibroma tumorigenesis.

Results

SCF expression in normal and neoplastic Schwann cells in vivo. Mast cell infiltration is a pathological feature of neurofibroma; however, the source of SCF mediating this mast cell chemotaxis in vivo remains unclear. Here, we first took advantage of the new Scf^{gfp} transgenic mice (*Scf* promoter-driven *Gfp*) (22) to evaluate the expression of *Scf* in normal and neoplastic peripheral nervous tissues. As SCF can be a secreted form of protein, the Scf^{gfp} provides a more precise identification of SCF-expressing cells compared with conventional SCF immunostaining. We observed SCF-expressing cells in normal peripheral nervous tissues in both dorsal root ganglia (DRG) and sciatic nerves (Figure 1, A and B). Immunostaining of S100β (a marker for both myelinating and nonmyelinating Schwann cells) confirmed that the SCF-expressing cells were Schwann cells in these normal peripheral nervous tissues (Figure 1, C and D). Next, we introduced Scf^{gfp} into a previously established plexiform neurofibroma genetically engineered mouse model (31) to determine the *Scf* expression in neurofibromas. We found that *Scf* expression was strongly detected in the plexiform neurofibroma tumor (Figure 1, E and F). Taken together, these results demonstrated that Schwann cells express *Scf* under both normal and neoplastic conditions, and importantly, suggested that Schwann cells could be the in vivo source of SCF to mediate mast cell infiltration in neurofibromas.

Tamoxifen-inducible plexiform neurofibroma mouse model. Human plexiform neurofibroma has been successfully recapitulated in genetically engineered mouse models with *Nf1* ablation in a number of Schwann cell–lineage Cre lines, including *Krox20-Cre* (31), *Dhh-Cre* (32), *P0A-Cre* (33), and *Plp-*Cre^{ERT2} (34). In this study, we employed our recently developed plexiform neurofibroma model with *Plp-*Cre^{ERT2} (34) with tamoxifen induction to address the role of tumor-derived SCF in neurofibroma development by introducing additional *Scf* depletion into *Nf1*-ablated Schwann cells.

Myelin-specific proteolipid protein (PLP) is expressed in myelinating Schwann cells from the precursor stage and lasts throughout their mature stages (35). In the *Plp-*Cre^{ERT2} plexiform neurofibroma model, we have previously demonstrated that Schwann cells are more susceptible to neurofibroma development when *Nf1* is ablated during the Schwann cell precursor or immature Schwann cell stage, but not the mature Schwann cell stage (34). Induction of *Nf1* ablation at the Schwann cell precursor stage (E12–E14) tends to result in a high rate of abortion due to tamoxifen toxicity. Therefore, in this work, we performed induction at the immature Schwann cell stage (newborn) to reduce mortality caused by induction.

In this study, we treated all newborn pups (both *Plp-*Cre^{ERT2+} and Cre^{-} controls) with 4-hydroxytamoxifen to induce *Nf1* (and *Scf*) ablation in Schwann cells (Supplemental Figure 1A; supplemental material available online with this article; https://doi.org/10.1172/JCI99424DS1). To validate the appropriateness of this new method, we performed a pilot experiment to evaluate the induction efficiency of *Plp-*Cre^{ERT2} by using *Nf1* genotyping, lineage tracing reporter *R26-LacZ*, and phenotype observation of plexiform neurofibroma formation. *Nf1* genotyping PCR showed a high efficiency of *Nf1* ablation (Supplemental Figure 1B). X-gal staining revealed a strong LacZ activity in peripheral nervous tissues in the DRG and sciatic nerves (Supplemental Figure 1C). Most importantly, in a 6-month-old $Nf1^{f/-}$ *Plp-*Cre^{ERT2} mouse, multiple plexiform neurofibromas were identified surrounding the spinal cord (Supplemental Figure 1D). Taken together, these results demonstrated that our 4-hydroxytamoxifen treatment can specifically and efficiently induce Cre recombination in Schwann cells. This system allows us to address the role of *Scf* depletion and *Nf1* heterozygosity in plexiform neurofibroma development.

The contribution of SCF and Nf1 heterozygosity to neurofibroma development. Next, we examined the contribution of tumor cell–derived SCF in neurofibroma genesis by introducing *Scf* mutation on top of $Nf1^{f/-}$ *Plp-*Cre^{ERT2} neurofibroma-bearing mice. We generated various combinations of *Scf* transgenes: (a) $Scf^{+/+}$ (WT), (b) $Scf^{f/+}$ (hemizygous deletion in Schwann cells), (c) $Scf^{+/gfp}$ (hemizygous deletion in all cells), and (d) $Scf^{f/gfp}$ (homozygous deletion in Schwann cells and hemizygous deletion in all other cells). This strategy allowed us to achieve a comprehensive comparison in order to better delineate the role of SCF in neurofibroma genesis.

In addition, *Nf1* heterozygosity has long been considered an important supportive factor to sustain the neurofibroma tumor microenvironment in *Krox20-Cre* mouse models (31), likely due to

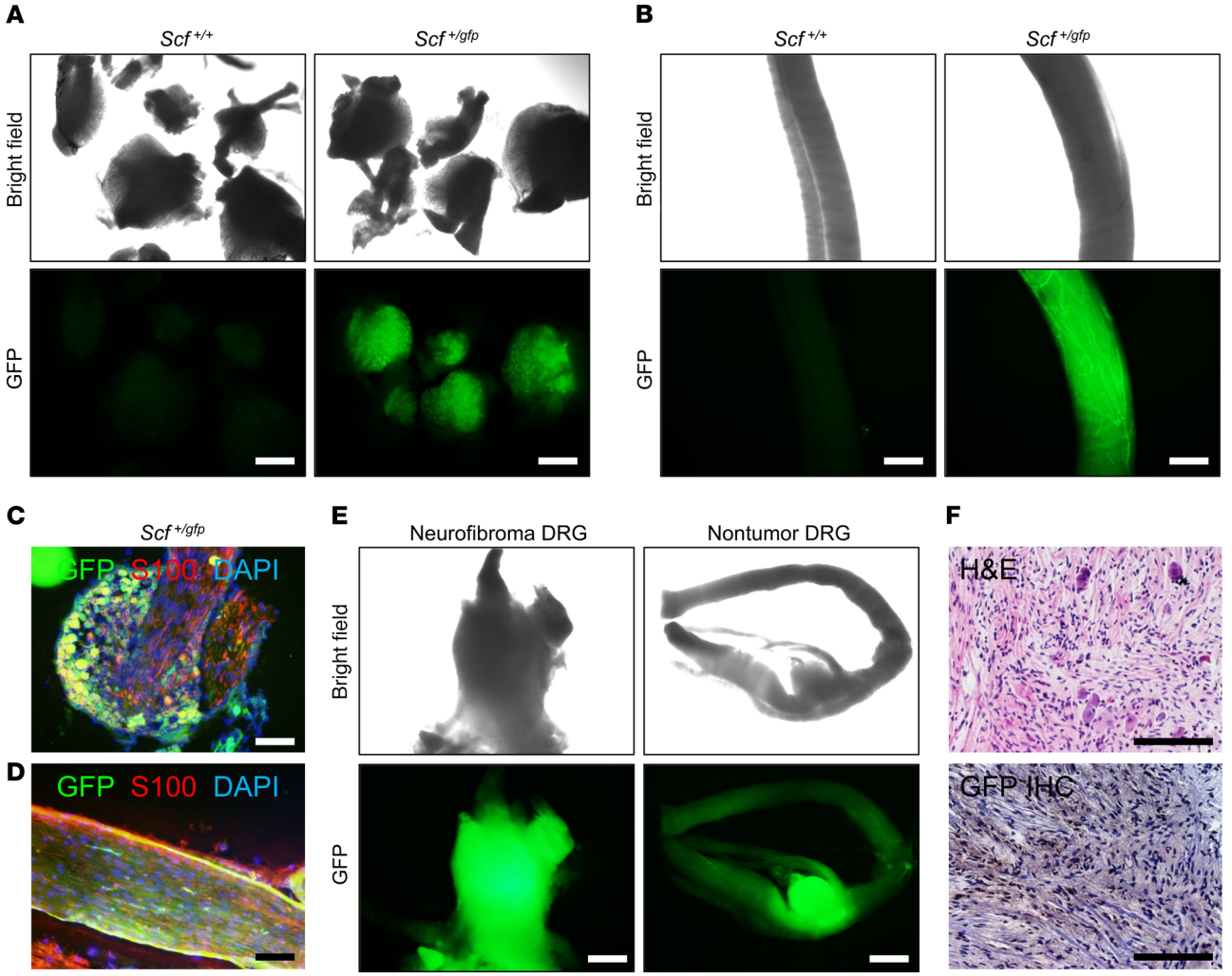

Figure 1. *Scf* expression in normal nervous tissues and neurofibroma tumors. (**A**) Scf^{gfp} identified *Scf* expression in DRG. (**B**) Scf^{gfp} identified *Scf* expression in sciatic nerve. (**C**) *Scf* expression in S100β$^+$ Schwann cells in DRG. (**D**) *Scf* expression in S100β$^+$ Schwann cells in sciatic nerves. (**E**) Scf^{gfp} identified *Scf* expression in DRG with spontaneous plexiform neurofibroma. (**F**) GFP immunohistochemical staining identified *Scf*-expressing cells (by Scf^{gfp}) in plexiform neurofibroma tumor tissue. Scale bar, 500 μm in **A**, **B**, and **E**. Scale bar, 100 μm in **C**, **D**, and **F**.

the contribution from $Nf1^{+/-}$ cells in the tumor microenvironment, especially mast cells (16). However, the requirement of the $Nf1^{+/-}$ microenvironment was not fully recapitulated in another neurofibroma model system by using *Dhh-Cre* (32), suggesting that *Nf1* haploinsufficiency might contribute to neurofibroma development in a context-dependent manner. Therefore, we also reevaluated the contribution of *Nf1* heterozygosity by comparing the tumor progression between $Nf1^{f/f}$ and $Nf1^{f/-}$ mice with *Plp-*Cre^{ERT2}.

In this study, we designed a comprehensive mouse breeding strategy that allowed us to examine the contribution of SCF and *Nf1* heterozygosity in neurofibroma development (Supplemental Figure 2A). A cohort size of 213 mice from 8 potential neurofibroma-bearing genotypes was enrolled in the survival study (Table 1). We also included a cohort of mice that do not carry *Cre* as controls. We employed Kaplan-Meier survival analyses to determine the tumor progression and death secondary to tumor burden among (a) *Plp-*Cre^{ERT2} (tumor-bearing) and Cre^- (no tumor) (Supplemental Figure 2B), (b) $Nf1^{f/-}$ and $Nf1^{f/f}$ background (Supplemental Figure 2C), and (c) $Scf^{+/+}$, $Scf^{f/+}$, $Scf^{+/gfp}$, and $Scf^{f/gfp}$ background (Supplemental Figure 2D) mice. These comparisons allowed us to determine the contribution of *Nf1* heterozygosity and tumor-derived SCF in the neurofibroma tumor microenvironment.

First, we evaluated the disease progression by comparing the tumor-bearing *Plp-*Cre^{ERT2} mice with Cre^- controls. In all groups with identical *Nf1* and *Scf* status, the survival rates of *Plp-*Cre^{ERT2} mice are significantly shorter than those of Cre^- controls (Figure 2A), confirming the tumor burden in neurofibroma-bearing *Plp-*Cre^{ERT2} mice (34, 36).

Second, we addressed the role of *Nf1* heterozygosity by comparing the disease progression between $Nf1^{f/-}$ and $Nf1^{f/f}$ background mice. We found that both $Nf1^{f/-}$ *Plp-*Cre^{ERT2} and $Nf1^{f/f}$ *Plp-*Cre^{ERT2} with paired *Scf* status mice succumbed to neurofibroma development (Figure 2A). However, mice in the $Nf1^{f/-}$ group died from tumor development much faster than those in the $Nf1^{f/f}$ group (Figure 2B). These findings revealed that *Nf1* heterozygosity is not absolutely required for neurofibroma development. However, inclusion of *Nf1* heterozygosity in nontumor cells significantly enhanced neurofibroma progression, suggesting that germline *Nf1* heterozygosity is

Table 1. The genotypes and number of mice enrolled in the plexiform neurofibroma study

Mouse	*n*
$Nf1^{f/-}$ $Scf^{+/+}$ Plp-Cre^{ERT2}	21
$Nf1^{f/-}$ $Scf^{f/+}$ Plp-Cre^{ERT2}	28
$Nf1^{f/-}$ $Scf^{+/gfp}$ Plp-Cre^{ERT2}	30
$Nf1^{f/-}$ $Scf^{f/gfp}$ Plp-Cre^{ERT2}	24
$Nf1^{f/f}$ $Scf^{+/+}$ Plp-Cre^{ERT2}	33
$Nf1^{f/f}$ $Scf^{f/+}$ Plp-Cre^{ERT2}	30
$Nf1^{f/f}$ $Scf^{+/gfp}$ Plp-Cre^{ERT2}	19
$Nf1^{f/f}$ $Scf^{f/gfp}$ Plp-Cre^{ERT2}	28
Total	213

a modifying factor for neurofibroma development and explaining the differential observations in previous reports (31, 32).

Finally, we determined the contribution of tumor-derived SCF in neurofibroma development. We compared the neurofibroma progression between various *Scf* statuses in tumor cells. In the common background of $Nf1^{f/-}$ Plp-Cre^{ERT2}, we found that *Scf* knockout ($Scf^{f/gfp}$) slightly prolonged the survival of mice; however, the difference only reached statistical significance when compared with $Scf^{+/gfp}$ ($P = 0.0191$), not to $Scf^{f/+}$ ($P = 0.0768$) or $Scf^{+/+}$ ($P = 0.1852$). In the common background of $Nf1^{f/f}$ Plp-Cre^{ERT2}, we found that *Scf* knockout ($Scf^{f/gfp}$) did not affect the survival of mice as compared with $Scf^{+/gfp}$ ($P = 0.5665$), $Scf^{f/+}$ ($P = 0.1924$), or $Scf^{+/+}$ ($P = 0.9817$). In short, these results reveal that depletion of SCF in neurofibroma Schwann cells only slightly influences its progression, suggesting the existence of other contributors to the neurofibroma tumor microenvironment. In addition, recent studies have shown that estrogen from females correlates with the prevalence of optic glioma (37, 38). Therefore, in this study, we also utilized our survival data set (Table 1) to compare the progression of neurofibromas between male and female mice, and we did not notice any significant difference (Supplemental Figure 3).

Loss of SCF does not affect neurofibroma anatomy or histopathology. To comprehensively analyze all of the developed tumors in the peripheral nervous tissues, we performed whole spinal cord extraction to identify paraspinal plexiform neurofibromas. We also included the *Rosa26-LacZ* lineage tracing reporter to mark Schwann cells. Therefore, after whole-mount X-gal staining, the plexiform neurofibroma tumors could be highlighted, providing an advantage for the clear identification of tumor locations and sizes. We performed the analyses for all 8 potential tumor-bearing groups (Table 1). To our knowledge, this is the first mouse plexiform neurofibroma study using whole spinal cord extraction in combination with X-gal staining enhancement as readout to quantify tumor burden.

Our results showed that plexiform neurofibromas can be found in every mouse among 8 potential tumor-bearing groups (Figure 3A), which is in agreement with our previous results showing all tumor-bearing groups had shortened survival due to tumor burden (Figure 2A). Based on their anatomical locations, these tumors can be classified into 3 groups: cervical, thoracic, and cauda equine. In general, these tumors were found at highest frequency in the cervical region (115 of 116 extracted spinal cords) and in the thoracic nerves (91 of 116 extracted spinal cords), but were less common in the cauda equine (39 of 116 extracted spinal cords). This trend of tumor preference applied to all groups and was not dependent on particular genotypes.

Although plexiform neurofibroma can develop in mice with various *Scf* and *Nf1* statuses, we were interested in understanding whether these genetic alternations would affect the pathological features of neurofibroma. Therefore, we performed analyses to evaluate neurofibroma derived from different genotypes. First, we characterized these tumors by H&E staining. We found that tumors from all groups shared classical pathological features of neurofibroma, including cellular disorganization with wavy nuclei, and high collagen content (Figure 3B). Second, we performed immunostaining for S100β, which is a common diagnostic marker for neurofibroma. Our results showed that $S100\beta^+$ Schwann cells were exhibited in a similar density and morphology among all groups (Figure 3C). Third, we quantified the tumor burden in each group. As mentioned previously, mouse plexiform neurofibromas were preferentially developed in cervical nerves. We therefore graded the tumor burden of cervical plexiform neurofibromas by their severity and prevalence in this region. In a total of 116 spinal cords, we found that the tumor burden was not statistically different between any 2 groups (Figure 3D). In summary, we did not notice any difference in plexiform neurofibroma histological structure due to the alterations of *Scf* and *Nf1* status in this study.

Schwann cells are the primary source of SCF for mast cell infiltration in neurofibromas. The key rationale behind our approach to deplete SCF in neurofibroma Schwann cells was to evaluate the impact of mast cells in the neurofibroma tumor microenvironment. Although we only observed a small difference in tumor progression by deleting Schwann cell–derived SCF, we reasoned it is necessary to quantify mast cell infiltration in these tumors.

Therefore, we compared the level of mast cell infiltration in neurofibroma tumor tissues with various *Scf* statuses by toluidine blue staining. We found that mouse neurofibroma tumors with normal *Scf* expression showed high levels of mast cell infiltration (Figure 4A), in line with the human neurofibroma pathological signatures (11–14). Strikingly, we found that mast cell density in neurofibroma is correlated to SCF expression in Schwann cells. Heterozygous loss of *Scf* ($Scf^{f/+}$ or $Scf^{+/gfp}$) lead to a partial decrease of mast cells (Figure 4B). On the other hand, complete loss of *Scf* ($Scf^{f/gfp}$) in Schwann cells resulted in a remarkable reduction of mast cells in tumors (Figure 4B). We found similar results in both $Nf1^{f/f}$ and $Nf1^{f/-}$ backgrounds (Figure 4B). Importantly, we found that in the case of hemizygous *Scf* loss ($Scf^{+/gfp}$), the reduction of mast cells was more drastic in $Nf1^{f/f}$ tumors than in $Nf1^{f/-}$ tumors. We reasoned that this could be due to hyperproliferation of the *Nf1* haploinsufficient mast cells as previously reported (29, 30). In brief, these results demonstrate that SCF from neoplastic Schwann cells is the key chemoattractant to drive mast cell chemotaxis in neurofibroma. However, removal of this source of SCF and mast cells was not sufficient to relieve tumor burden (Figure 3).

Neurofibroma is associated with high levels of macrophage infiltration regardless of SCF status. The observation that neurofibroma progression was only slightly affected when mast cells were

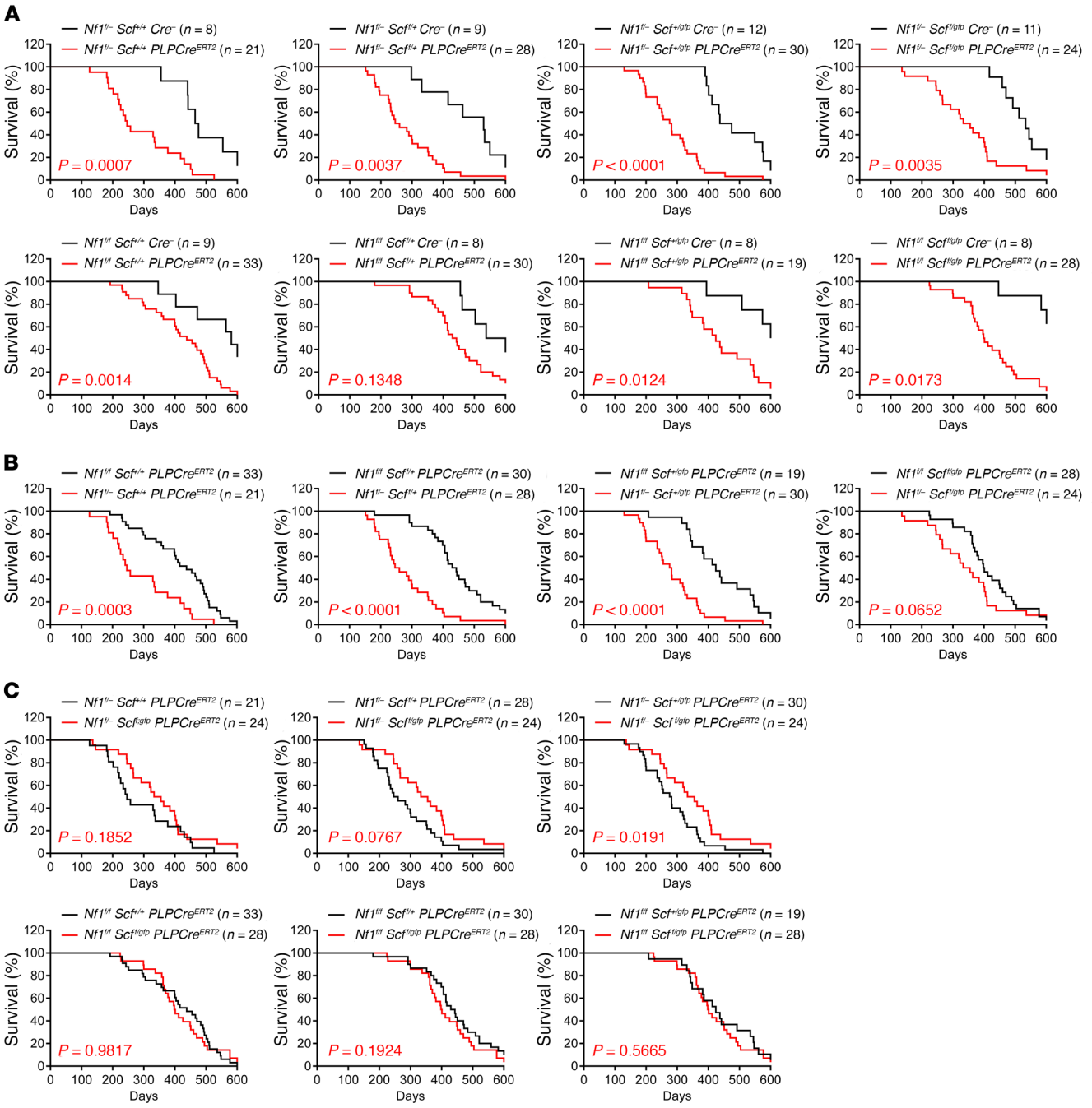

Figure 2. Contributions of *Nf1* heterozygosity and SCF to neurofibroma progression. The speed of neurofibroma progression was determined by the survival of mice. (**A**) Survival comparison between neurofibroma-bearing (*PlpCre*^{ERT2}) and tumor-free (no *Cre*) mice. (**B**) Survival comparison between neurofibroma-bearing mice with germline homozygous *Nf1* (*Nf1*$^{+/+}$) and heterozygous *Nf1* (*Nf1*$^{+/-}$) status. (**C**) Survival comparison between neurofibroma-bearing mice with the following variable *Scf* status: (1) *Scf*$^{+/+}$, WT; (2) *Scf*$^{f/+}$, hemizygous deletion in Schwann cells; (3) *Scf*$^{+/gfp}$, hemizygous deletion in all cells; and (4) *Scf*$^{f/gfp}$, homozygous deletion in Schwann cells and hemizygous deletion in all other cells. The number of mice in each group ranged from 19–30 as labeled in each individual figure. The statistics were performed by Kaplan-Meier estimator with log-rank test. In this figure, the same survival curves from *Nf1*$^{f/-}$ *Scf* $^{f/gfp}$ *Plp-Cre*^{ERT2} and *Nf1*$^{f/f}$ *Scf* $^{f/gfp}$ *Plp-Cre*^{ERT2} double knockout mice were presented in **A**–**C** to compare the survival between different genotype cohorts.

removed from the tumor microenvironment suggested that mast cells are a modifier rather than a driver in neurofibroma development (Figure 2C). This is in alignment with the human clinical findings that only a portion of plexiform neurofibromas in patients with NF1 showed partial response to KIT inhibitor imatinib mesylate (39). The results from both preclinical and clinical studies suggested that targeting mast cells alone is not potent enough to efficiently relieve neurofibroma burden, suggesting the existence of additional mediators in the neurofibroma microenvironment. Therefore, we evaluated other inflammatory signatures in these neurofibroma tumors. Macrophage is another type of inflammatory cell found in neurofibroma (40, 41). Similar to mast cells,

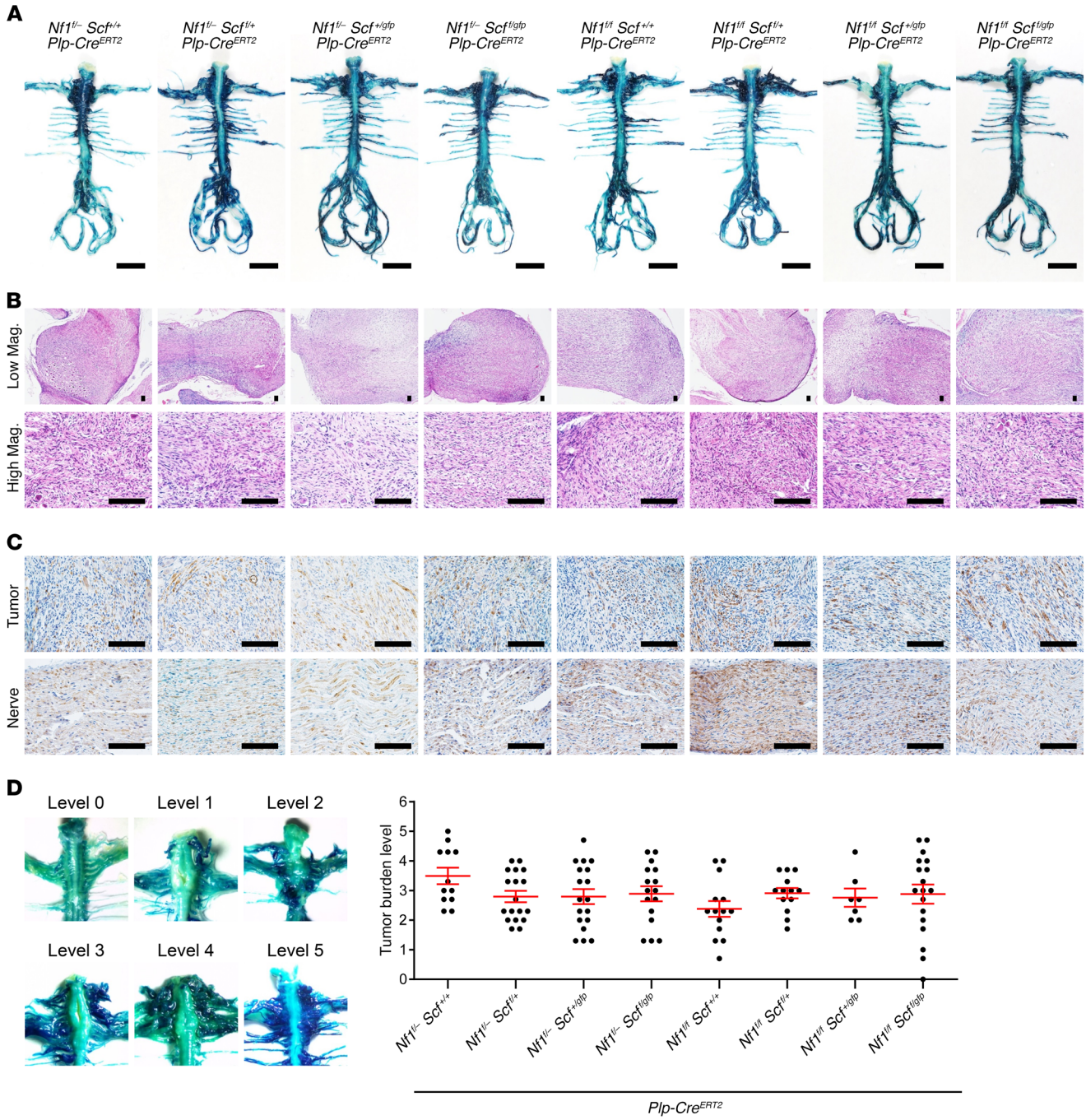

Figure 3. Contributions of *Nf1* heterozygosity and SCF to neurofibroma development. (**A**) The structure of whole spinal cord from neurofibroma-nearing mice. X-gal staining marks *Plp*-lineage Schwann cells. Plexiform neurofibromas were highlighted as enlarged DRGs. A representative image in each group was selected from a 10- to 12-month-old mouse as shown in Supplemental Figures 4–11. (**B**) The histology of cervical plexiform neurofibromas. (**C**) S100β immunohistochemical staining for Schwann cells in the tumors and nontumor nerves. (**D**) Quantification of the severity of plexiform neurofibroma by a reference grading scale in the left panel. No statistically significant difference was identified by comparing any 2 groups. Cervical tumors in left panel are representative images for each level (0–5) selected from 116 whole spinal cords as shown in Supplemental Figures 4–11. For **A**–**C**, representative images were compared from mice at similar ages (10–12 months) in each group. Statistics were performed by 1-way ANOVA. Data are mean ± SEM. Scale bar, 1 cm in **A**. Scale bar, 100 μm in **B** and **C**.

macrophages are recruited to neurofibroma by tumor-derived chemoattractant macrophage CSF1 (40).

We therefore determined macrophage density by staining with macrophage marker Iba1 (40). We found that macrophages were present at high densities in neurofibroma tumors in all groups; these cells are diffused across the entire tumor region (Figure 5A). Macrophages can polarize into different subtypes of cells depending on the context of the microenvironment (42). Therefore, we further phenotyped these macrophages using markers for M1 (proinflammatory) and M2 (protumorigenic) macrophages. Our

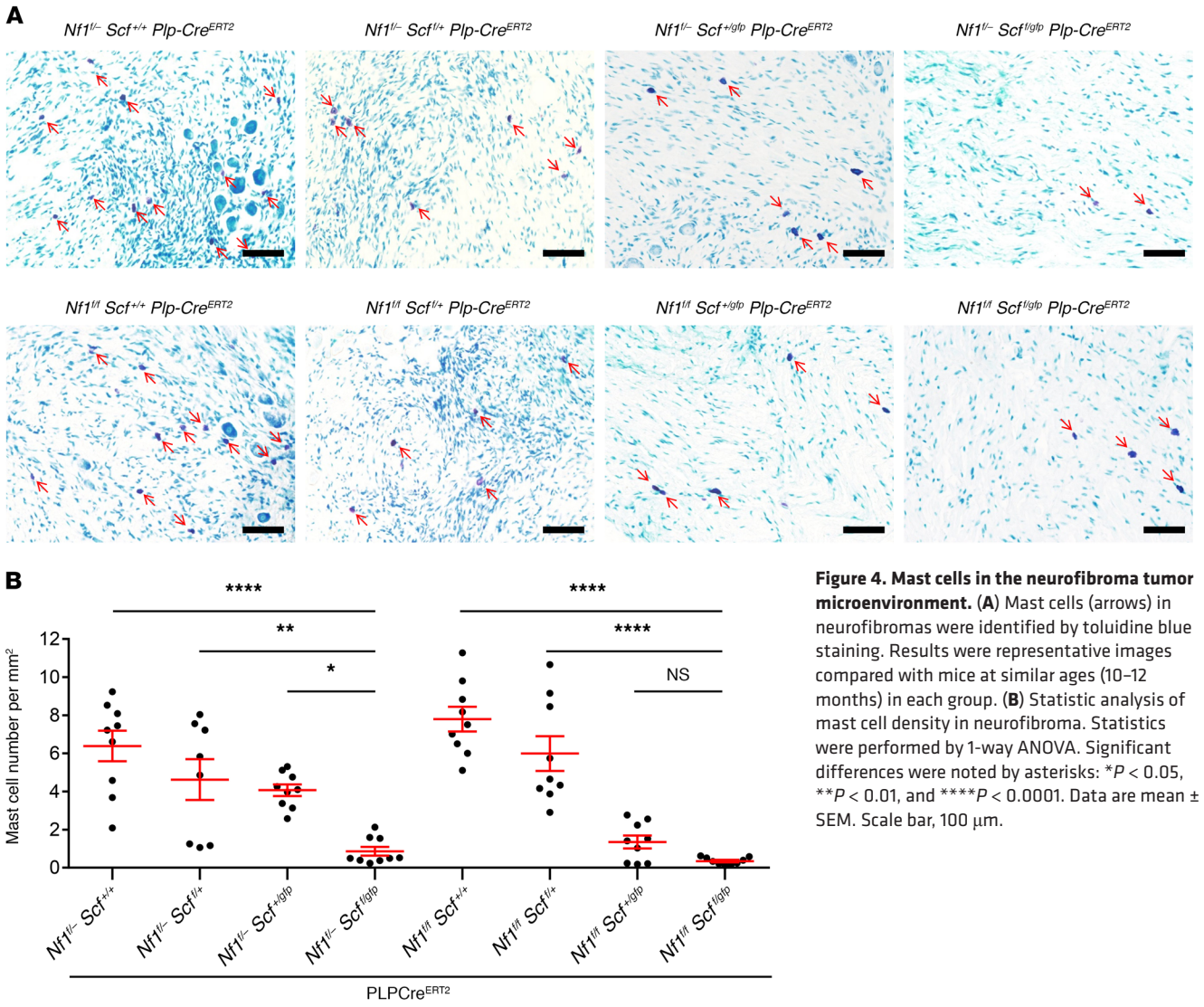

Figure 4. Mast cells in the neurofibroma tumor microenvironment. (**A**) Mast cells (arrows) in neurofibromas were identified by toluidine blue staining. Results were representative images compared with mice at similar ages (10–12 months) in each group. (**B**) Statistic analysis of mast cell density in neurofibroma. Statistics were performed by 1-way ANOVA. Significant differences were noted by asterisks: $^{*}P < 0.05$, $^{**}P < 0.01$, and $^{****}P < 0.0001$. Data are mean ± SEM. Scale bar, 100 μm.

results showed that macrophages in neurofibromas are predominantly iNOS^{+} M1 macrophages (Figure 5B) rather than mannose receptor^{+} M2 macrophages (Supplemental Figure 12), suggesting an inflammatory status in neurofibromas. We also noticed the presence of a small number of CD3^{+} T lymphocyte clusters in the tumors (Supplemental Figure 13). Unlike macrophages, however, T lymphocytes in neurofibromas were in groups and at a much lower density. In contrast to the tumor areas, our data showed that only a small number of M1 macrophages are detected in nearby nontumor nerves (Figure 5), suggesting a correlation between inflammation and neurofibroma formation. Furthermore, we also found that macrophage levels were not affected by the alternations of *Scf* or *Nf1* heterozygosity status (Figure 5). This finding partly explains the limited efficacy of our antitumor approach by removing SCF and mast cells (Figures 2 and 3).

Paraspinal plexiform neurofibroma preferentially developed at cervical and thoracic T5–T8 nerves. In our whole spinal cord extraction analysis in a cohort of 116 mice, we found that paraspinal plexiform neurofibromas were most prevalent in cervical nerves (Figure 3A, Supplemental Figures 4–11, and Supplemental Table 1). Plexiform neurofibromas can also be found in thoracic nerves and in the cauda equina, but in much lower frequencies (Figure 3A, Supplemental Figures 4–11, and Supplemental Table 1). After analyzing the thoracic neurofibromas in 116 spinal cords, we noticed that among 13 pairs of thoracic nerves, plexiform neurofibromas appeared to preferentially develop in particular areas. We therefore performed quantification analysis to determine the number and sizes of tumors formed in each thoracic nerve.

We found that all 8 different groups of tumor-bearing mice gave rise to a similar trend of thoracic neurofibroma formation (Figure 6 and Supplemental Figure 14). This pattern can be summarized as follows (a) among 13 pairs of thoracic nerves, tumors only develop from T1 to T9, no tumors were from T10 to T13 (Figure 6), (b) tumors with the largest average size were located at T5 to T8 (Figure 6), and (c) in a total of 188 thoracic tumors, tumors were most frequently identified in T7 (40%), and the T5–T8 tumors take up 69% prevalence in all thoracic tumors (Supplemental Figure 14).

Taken together, these results indicate that the cervical nerves and the thoracic nerves at T5–T8 are the "hot zones" for paraspi-

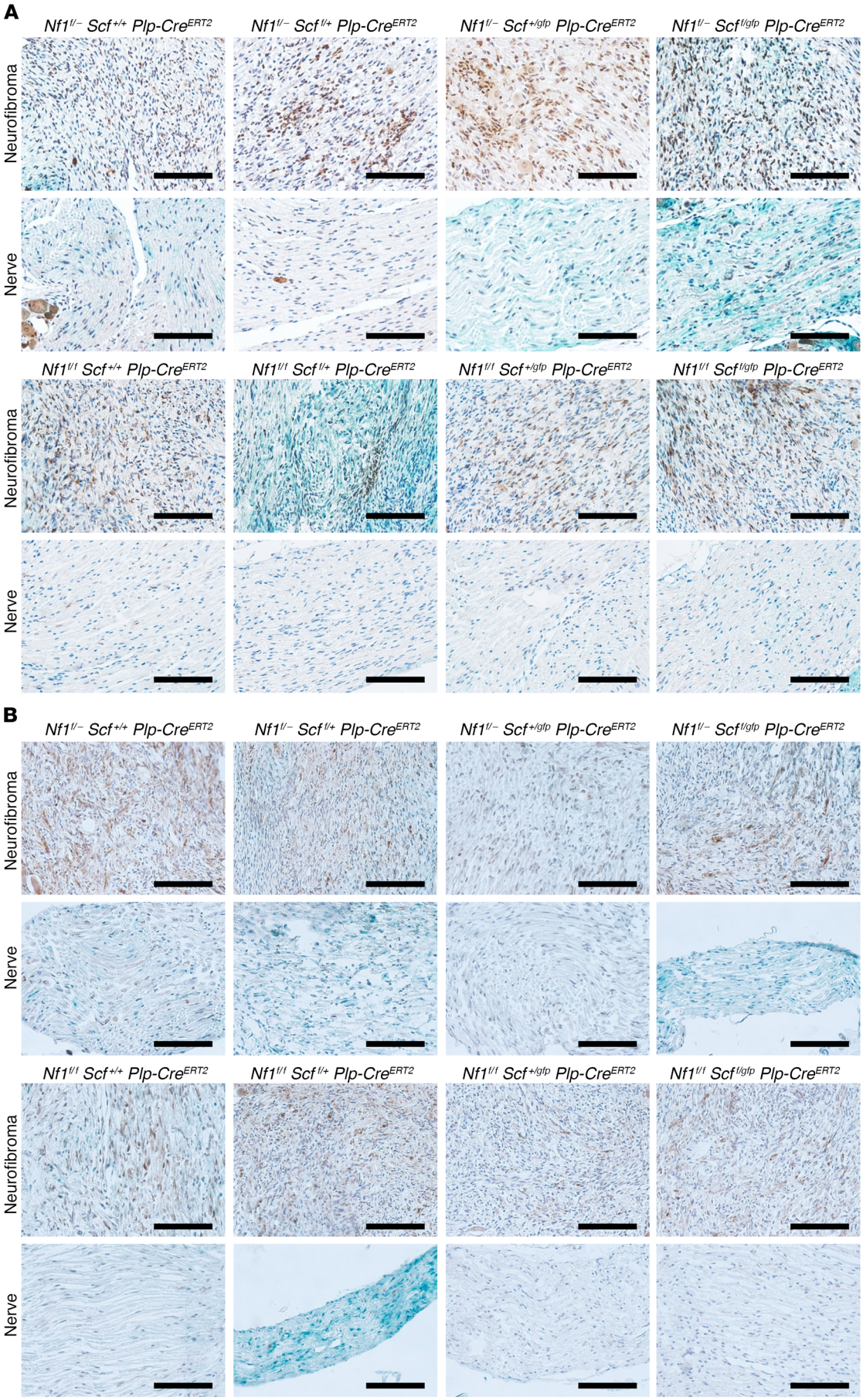

Figure 5. Macrophages in the neurofibroma tumor microenvironment. Iba1 (**A**) and iNOS (**B**) immunohistochemical staining for macrophages in the cervical plexiform neurofibroma tumor and nearby nontumor nerve regions. Note the density difference of positive cells in tumors and nerves. Representative images are shown from mice with similar ages (10–12 months) in each group (n = 3). Scale bars, 100 μm.

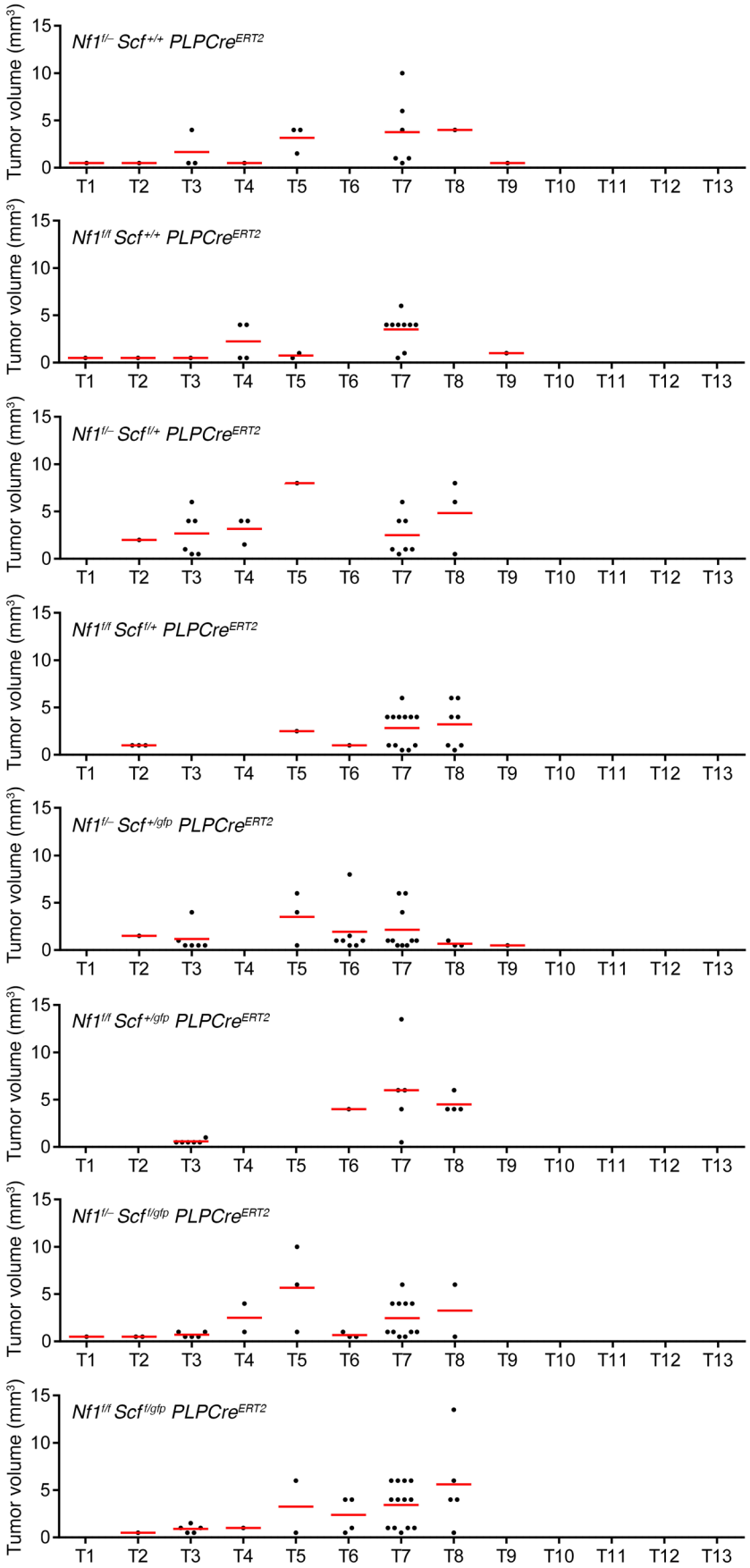

Figure 6. The prevalence of thoracic neurofibroma in different thoracic nerves. The number and sizes of thoracic neurofibromas in different thoracic locations in different groups of neurofibroma-bearing mice. Figure represents the sizes and locations of each tumor with means. Note the high tumor prevalence in T5–T8 (n = 7–18 mice per group).

nal plexiform neurofibroma formation. Interestingly, in mice, the cervical vertebras and the T5–T8 vertebra, which are located in the middle of the thoracic spine, flex and extend more than any other part of the spine. Therefore, we speculate that these nerves and DRGs may be more prone to injury, which might be related to the observations of M1 macrophages and T lymphocytes in neurofibromas (Figure 5 and Supplemental Figure 13).

Tumorous Schwann cell–derived SCF is dispensable for neurofibroma development in the transplant tumor model. In our genetically engineered mouse models, we showed that SCF expression in tumorous Schwann cells is not absolutely required for neurofibroma development (Figures 2 and 3). Although we have shown effective tamoxifen induction efficiency by genotyping and X-gal staining (Supplemental Figure 1), we still cannot rule out the possibility that there were a small portion of Scf^{fl} alleles in Schwann cells that were not completely ablated due to the efficacy limitation of the Cre/Flox recombination system.

We therefore employed another neurofibroma model we established previously (43). That system utilizes *Nf1*-ablated skin-derived precursors (SKPs) as the cell of origin for neurofibroma in nude mice orthotopic allograft transplantation, where the *Nf1*-ablated SKPs develop into bona fide neurofibroma when transplanted into sciatic nerves. In the present study, we took advantage of that system to address the role of tumorous SCF in neurofibroma development by examining the tumorigenicity of $Nf1^{\Delta f/\Delta f}$ $Scf^{gfp/gfp}$ (*Nf1/Scf*-DKO) SKPs. The Scf^{gfp} allele is functionally equivalent to *Scf* straight knockout; therefore, biallelic Scf^{gfp} confers an absolute loss of SCF (22).

We first examined the *Scf* expression in SKPs by taking advantage of Scf^{gfp} as a reporter. We found that SKP spheres express *Scf* (Figure 7A). To ensure this SCF expression was in the neural crest–derived stem cells in the SKPs, we stained neural crest marker Nestin and found that Nestin$^+$ cells were colocalized with GFP in monolayered SKP cells (Figure 7B). Next, we generated SKPs from mice with the following 3 genotypes: (a) $Nf1^{f/f}$ $Scf^{+/+}$, (b) $Nf1^{f/f}$ $Scf^{+/gfp}$,

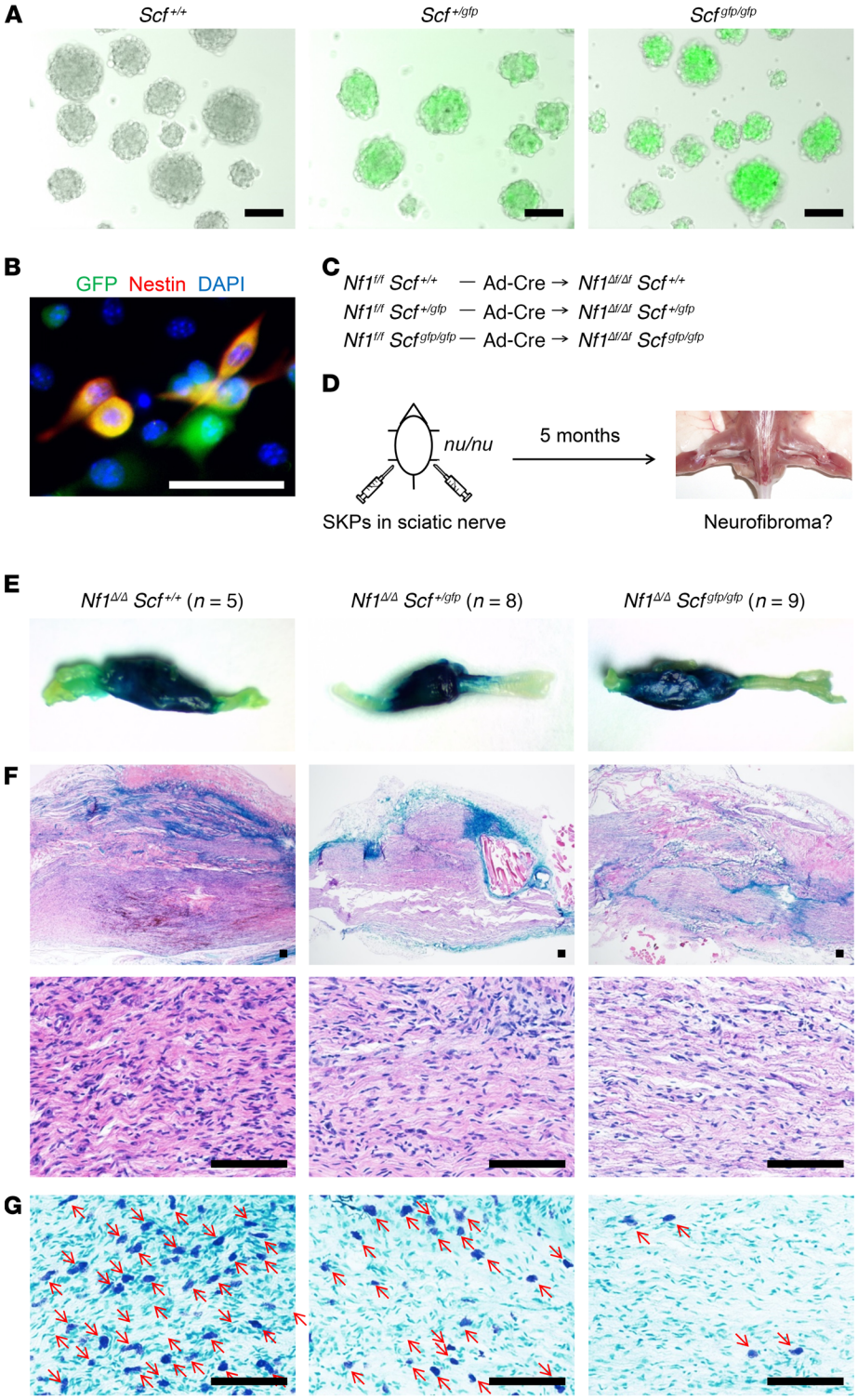

Figure 7. Contribution of tumor-derived SCF in SKP transplantation neurofibroma model. (**A**) *Scf*^{gfp} reporter identified *Scf* expression in the SKP spheres. (**B**) Scf expression (determined by *Scf*^{gfp}) in the Nestin$^+$ neural crestlike stem cells in the SKPs. (**C**) The strategy of generation of *Nf1/Scf* DKO SKPs and controls. (**D**) Illustration of SKP transplantation in sciatic nerves in nude mice for neurofibroma development. (**E**) The observation of sciatic nerves with LacZ staining (marked by dark blue color) after SKP transplantation. (**F**) The histology of sciatic nerves at low magnification (×40, upper panel) and high magnification (×400, lower panel). (**G**) Toluidine blue staining for mast cells. In **E**–**G**, results were representative from 5–9 tumors, as labeled. Scale bars, 100 μm in **A**, **F**, and **G**. Scale bar, 50 μm in **B**.

and (c) *Nf1*$^{f/f}$ *Scf*$^{gfp/gfp}$. We then infected these SKPs by adenovirus-carrying Cre recombinase (Ad-CMV-Cre) to ablate their *Nf1* alleles and obtain the following SKPs: (a) *Nf1*$^{Δf/Δf}$ *Scf*$^{+/+}$ (*Nf1*-KO), (b) *Nf1*$^{Δf/Δf}$ *Scf*$^{+/gfp}$, and (c) *Nf1*$^{Δf/Δf}$ *Scf*$^{gfp/gfp}$ (*Nf1/Scf*-DKO) (Figure 7C). These SKPs were transplanted into the sciatic nerves in nude mice and harvested 5 months after transplantation (Figure 7D).

The rationale of this experiment was to determine whether *Nf1/Scf*-DKO and *Nf1*-KO will show different neurofibroma tumorigenicity due to the lack of SCF expression in the neoplastic Schwann cells. We also included *Nf1*$^{Δf/Δf}$ *Scf*$^{+/gfp}$ SKPs as a partial SCF loss control. We found that SKPs from all 3 groups gave rise to neurofibromas with similar sizes (Figure 7E). Histologically, neurofibromas derived from all groups showed similar tissue structure (Figure 7F). However, the levels of infiltrated mast cell density in neurofibromas were strongly correlated to the *Scf* status in the transplanted SKP, where the *Nf1*$^{Δf/Δf}$ *Scf*$^{+/+}$ tumor had

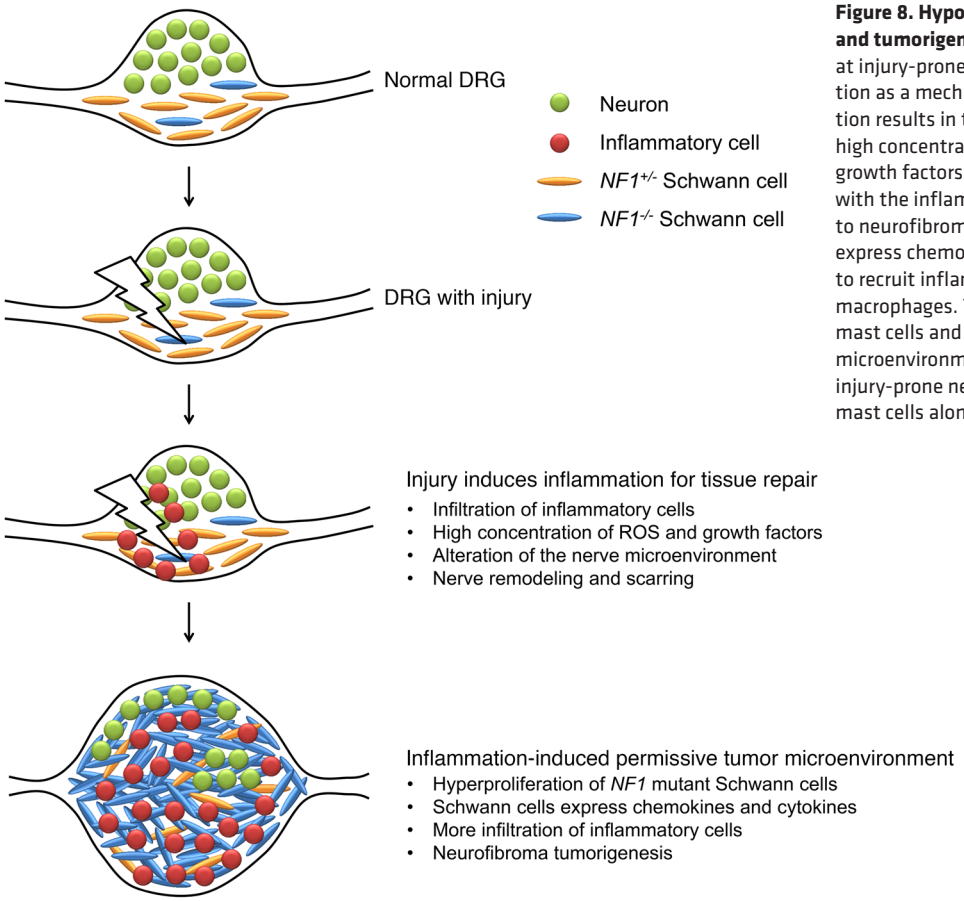

Figure 8. Hypothetical model of neurofibroma initiation and tumorigenesis. Neurofibroma occurs more commonly at injury-prone nerves. Nerve injury induces inflammation as a mechanism of tissue repair. Nerve inflammation results in the infiltration of inflammatory cells and high concentrations of reactive oxygen species (ROS) and growth factors. *NF1* mutant Schwann cells may interplay with the inflammatory microenvironment that contributes to neurofibroma tumorigenesis. Tumorous Schwann cells express chemokines and cytokines, such as SCF and CSF1, to recruit inflammatory cells, including mast cells and macrophages. This model may explain the presence of mast cells and macrophages in the neurofibroma tumor microenvironment, the high neurofibroma frequency in injury-prone nerves, and our observation that removal of mast cells alone is not sufficient to relieve tumor burden.

the highest level, $Nf1^{\Delta f/\Delta f}$ $Scf^{+/gfp}$ tumor had the moderate level, and $Nf1^{\Delta f/\Delta f}$ $Scf^{gfp/gfp}$ tumor had the lowest level (Figure 7G). This finding confirmed that mast cell infiltration in neurofibroma in vivo is primarily dependent on the SCF expression from tumorous Schwann cells; however, the differences in mast cell infiltration do not alter neurofibroma tumorigenesis. These results are in agreement with our previous mouse model experiments presented earlier (Figures 2–4).

Discussion

Neurofibroma is a benign peripheral nerve sheath tumor that can cause severe disfiguring in a majority of patients with NF1. Fighting neurofibroma has been a continuous effort with limited success. In this study, we aimed to understand the important interactions between tumorous Schwann cells and their microenvironmental cells by employing new genetically engineered mouse models. We found that (a) tumorous Schwann cells are the primary source of SCF that mediates mast cell chemotaxis in neurofibroma but that mast cell density does not correlate with tumor burden, (b) paraspinal neurofibroma initiation appears to be more prevalent in certain areas of the spine that are prone to nerve injury, such as the cervical or T5–T8 DRGs, and (c) *Nf1* heterozygosity plays a key role in tumorigenesis, whereas it is not absolutely required for but can modify neurofibroma tumorigenesis.

It is widely recognized that biallelic *Nf1* loss is the key fundamental requirement for neurofibroma initiation (2–7). If biallelic *Nf1* loss is the only requirement to initiate neurofibroma tumorigenesis, all *Nf1*-ablated Schwann cells should harbor the same chance to form tumors, and therefore tumors should develop in a homogenous manner in all peripheral nerves under the efficient induction condition that we have achieved (Supplemental Figure 1). However, our results clearly demonstrate the preferential sites for plexiform neurofibroma in the cervical nerves and in the thoracic T5–T8 nerves, pointing to the requirement of other factors, whether intrinsic or extrinsic, in addition to *Nf1* loss for neurofibroma development (Figure 8).

In mice, the joints in cervical vertebras and in the mid-thoracic vertebras are most flexible to allow head rotation and walking. Therefore, their associated nerves and DRGs may be more prone to injury, leading to higher neurofibroma prevalence, as nerve injury has been associated with neurofibroma development (44, 45). Our observation that cervical nerves serve as a "hot zone" for plexiform neurofibroma in this mouse model appears to mimic similar observations in human NF1 studies (46, 47). We hypothesize that physical motion could lead to minor but repetitive nerve injuries surrounding these vertebras compared with the nerves near other less-active spinal vertebras. Tissue injuries are usually accompanied by inflammation as a mechanism for tissue repair. Repetitive inflammation has been generally recognized as a stimulating factor for neoplasia, primarily due to the reactive oxygen species–induced DNA mutations and the high concentrations of cytokines and growth factors from infiltrating inflammatory cells (Figure 8) (48, 49).

In addition to mast cells, macrophages are another type of inflammatory cell frequently found in neurofibromas. Macro-

phages can polarize into different types of cells depending on the context of environmental cues (42). M1 macrophages are phagocytic and they are often present in inflammatory tissue to remove the damaged cells. On the other hand, M2 macrophages are protumorigenic; they are associated with the hyperproliferation of neoplastic cells. A recent genomic profiling revealed that macrophages in neurofibromas showed stronger M1 signatures than M2 (41). This finding is in agreement with our discovery and suggests a continuous inflammation in the neurofibroma microenvironment. Taken together with our discovery that cervical nerves and the thoracic T5–T8 nerves are the hot spots for neurofibromas, it would be important to understand through future studies whether this macrophage infiltration is associated with nerve injury.

If nerve injury is a modifying factor for neurofibroma initiation in addition to *Nf1* loss, the presence of mast cells in neurofibromas might be one of the many inflammatory cell infiltrations (including macrophages and others) that accompany nerve injury, whether mechanical or molecular, explaining the limited efficacy in the attempt to reduce mast cell infiltration to prevent neurofibroma development in this study (Figures 2 and 3). Therefore, future clinical trials utilizing dual inhibitions for both mast cells and macrophages may be much more effective for this tumor. On the other hand, although we found that mast cell infiltration in neurofibromas was markedly diminished when SCF was depleted in Schwann cells, it is also possible that the mast cell number did not fall below a required threshold level to prevent tumor development. Thus, Schwann cell SCF may be a crucial but not the only source of SCF for recruiting mast cells, suggesting the contribution of SCF from other cell types in the neurofibroma tumor microenvironment. This might be why targeting the KIT receptor on mast cells, whether via genetic ablation or pharmacological inhibition with imatinib, is effective in preventing neurofibroma development (16, 39). Future experiments to utilize mice with mast cell–, fibroblast-, or endothelial cell–specific Cre to explore the role of SCF from other cell types in the neurofibroma microenvironment would help to delineate the absolute requirement of SCF within the neurofibroma microenvironment for tumor initiation.

In summary, our study highlighted the contribution of inflammation (possibly due to nerve injury) in neurofibroma initiation (Figure 8). Here we propose that prevention of repetitive nerve injury (both physiological and traumatic) or blocking of nerve inflammation could be a new strategy to manage neurofibroma growth. This concept is partly supported by the preliminary success of long-term treatment of ketotifen in a human (20), as it is not only in possession of antihistamine from mast cells but also antiinflammatory activities (50). Another similar success in mouse models was achieved by treatment with PLX3397 (40), a dual inhibitor of KIT and CSF1R, which could simultaneously block mast cells and macrophages. Thus, the findings in our study address the contributions of tumor-derived SCF, inflammation, and germline *Nf1* heterozygosity to neurofibroma development and provide insights for the design of future neurofibroma therapies in targeting its tumor microenvironment.

Methods

Mice. The $Nf1^{fl}$ (51), $Nf1^{-}$ (52), Scf^{fl} (22), $Scf^{\delta fp}$ (22), and *Plp-Cre*^{ERT2} (53) mice have been reported in previous literatures. The *Rosa26-LacZ* (54) lineage tracing reporter was obtained from The Jackson Laboratory and included in all the mice in this study. Mice were maintained on a 129/SvEv and C57BL/6 mixed background. Male and female mice were nonselectively included in this study. The genotype and age of mice were indicated in each experiment.

4-hydroxytamoxifen induction. The *Plp-Cre*^{ERT2} is a tamoxifen inducible Cre system. In order to induce Cre recombinase expression in the *Plp*-lineage Schwann cells in mice, we injected 40 μg of 4-hydroxytamoxifen subcutaneously into each P0–P2 pup. Efficient induction was validated in Supplemental Figure 1.

Plexiform neurofibroma progression analysis. In this study, all the mice were subjected to the same dose of 4-hydroxytamoxifen induction at the same stage of age. Therefore, we assumed that the initiation and progression of spontaneous plexiform neurofibroma in each individual neurofibroma-bearing mouse shared the same probability; the only variable is their genotype. Mice with benign plexiform neurofibroma are generally asymptomatic during their early life. Along the tumor progression, the enlarged tumors could compress the DRG and spinal cord, leading to impaired peripheral and central nervous signaling. In the end stage of disease development, mice are commonly skinny and present with limpness, hunched back, rough coat, and shallow breathing. When mice were reported sick by the Animal Research Center, we euthanized them and extracted the entire spinal cord for histology analysis. The date of euthanasia was documented for the length of survival. Some mice died before we could perform dissection. Their dates of death were also documented for survival analysis; however, their tissues were excluded from our histology analyses for quality purposes. Overall, mice with plexiform neurofibroma live about 6 to 18 months of age. Mouse survival analysis was compared by Kaplan-Meier statistics.

Whole spinal cord extraction. Mice were anesthetized by intraperitoneal injection of a mixture of 30 mg/ml ketamine and 4 mg/ml xylazine solution at a dose of 100 μl per 25 g. Total body perfusion was performed by transcardial injection of 20 ml PBS and then 20 ml of 4% paraformaldehyde. The vertebras with connecting dorsal ribs, pelvis, and femurs were excised. The extraction of spinal cord and connecting peripheral nerves was performed by carefully dissecting out the muscles and bones under a dissection microscope.

LacZ staining. When the whole spinal cord was extracted, it was briefly fixed in 4% paraformaldehyde for 30 minutes followed by rinsing in PBS. LacZ staining on the spinal cord was performed in X-gal solution (1 mg/ml 4-chloro-5-bromo-3-indolyl-β-galactoside, 4 mM potassium ferrocyanide, 4 mM potassium ferricyanide, 2 mM magnesium chloride in PBS) at 37°C for overnight. X-gal–stained spinal cord was fixed in 10% formalin overnight and then imaged.

Plexiform neurofibroma quantification. For cervical neurofibromas, the tumors tend to present in a diffuse pattern due to the tight proximity of cervical nerves. Therefore, it was difficult to grade the size of independent tumor in this region. To overcome this difficulty, we established a tumor burden scale (Figure 3D) to quantify the relative severity and prevalence of cervical neurofibroma in each mouse, as follows: level 0, no tumor was detected; level 1, tumors formed in less than 20% of cervical nerves; level 2, tumors formed in 20%–40% of cervical nerves; level 3, tumors formed in 40%–60% of cervical nerves; level 4, tumors formed in 60%–80% of cervical nerves; level 5, tumors formed in more than 80% of cervical nerves. Data represent the averages of 3 independent blind-grading experiments performed by different neuro-

fibroma research scientists. For thoracic neurofibromas, we identified the tumors by the size of DRG, which is equal or greater than 1 mm × 1 mm. The volume of each tumor was calculated by the formula (length) × (width)^2 × 0.5.

Histology analysis. For histology analysis, visible plexiform neurofibroma was excised from the spinal cord and then subjected to tissue processing and paraffin embedding. Tissue block was sectioned at 5-μm thickness. H&E staining was performed according to the manufacturer's protocol (StatLab).

Immunostaining. Immunostaining was performed on paraffin sections after deparaffinization, rehydration, and antigen retrieval. The primary antibodies used in this study were S100β (Dako, Z0311), GFP (Aves, 1020), Iba1 (Wako, 019-19741), iNOS (Abcam, ab15323), mannose receptor (Abcam, ab64693), CD3 (Abcam, ab16669), and Nestin (Abcam, ab24692). For immunofluorescent staining, the primary antibodies were detected by secondary antibodies conjugated with Cy3 (Jackson ImmunoResearch), and nuclei were counterstained with DAPI (Vector Laboratories). For immunohistochemical staining, the primary antibodies were detected by biotin-conjugated secondary antibodies followed by streptavidin conjugated with DAB (Vector Laboratories).

Toluidine blue staining. Toluidine blue staining for mast cells was performed on paraffin sections after deparaffinization and rehydration. Tissue was stained with 0.5% toluidine blue solution (Acros Organics) for 5 minutes and rinsed by water. Then tissue was dehydrated in increasing concentrations of ethanol solutions and xylene before mounting. This dye highlights mast cells in purple, whereas other cells were in blue.

SKP isolation and Nf1 ablation by adenoviral Cre. SKP isolation was described previously (55). Briefly, dorsal skin was excised from P0–P2 neonatal mouse pups followed by the removal of adipose and muscle tissues. The skin was rinsed by HBSS (Invitrogen) and then chopped to 2 mm to 3 mm in size by sterile technique. To isolate single cells from the skin, tissue was gently shaken in 0.5% collagenase I (Invitrogen) at 37°C for 1 hour. Tissue underwent pipetting several times to facilitate tissue dissociation. Undissociated tissue was removed by 70-μm cell strainer. Cells in suspension were pelleted and then washed with serum-free DMEM/F12 media (Invitrogen). Skin cells were plated at a density of 20 cells/μl on ultra-low attachment plates (Corning) in SKP proliferation media (DMEM/F12 containing penicillin/streptomycin [0.1%], fungizone [40 μg/ml], B27 [without vitamin A], epidermal growth factor [20 ng/ml], and basic fibroblast growth factor [40 ng/ml]) (Sigma-Aldrich). SKPs formed spheres by the time of culture. SKPs were fed by fresh media every 3 to 4 days and passaged every 7 days. Ablation of *Nf1* was performed by Ad-CMV-Cre infection as previously described (36).

SKP transplantation in nude mice. Athymic nude mice were anesthetized as described above. Dissociated SKP single cells (5×10^5) were resuspended in 40 μl of L15 medium (Gibco) and then injected into the sciatic nerve in athymic nude (*nu/nu*) mice as previously described (36). Neurofibromas derived from SKPs were harvested 5 months after SKP transplantation.

Statistics. All statistical analyses in this study were performed using Prism7 (GraphPad). For mouse survival analysis, the Kaplan-Meier estimator with log-rank statistical test was employed. Multiple group comparison was performed by 1-way ANOVA test. Data are mean ± SEM. Significant differences are noted by asterisks: $^*P < 0.05$, $^{**}P < 0.01$, $^{***}P < 0.001$, and $^{****}P < 0.0001$.

Study approval. Mouse care and use in this study were approved by the IACUC at the University of Texas Southwestern Medical Center. The approved protocol numbers are 2011-0156 and 2017-102108.

Author contributions

CPL, LQL, and DWC designed the studies. CPL, RCB, JPB, ZC, JM, ET, and YW performed the experiments. CPL acquired the data. CPL and LQL analyzed the data and wrote the manuscript.

Acknowledgments

We thank all members of the Le lab for helpful suggestions and discussions. We also thank Sean Morrison (University of Texas Southwestern Medical Center), Ueli Suter (Swiss Federal Institute of Technology), and Luis Parada (Memorial Sloan Kettering Cancer Center) for sharing *Scf*, *Plp*, and *Nf1* mice, respectively. CPL is a recipient of the Young Investigator Award from the Children's Tumor Foundation and the Career Development Award from the Dermatology Foundation. LQL holds a Career Award for Medical Scientists from the Burroughs Wellcome Fund and the Thomas L. Shield, M.D., Professorship in Dermatology. This work was supported by funding from the National Cancer Institute of the NIH (grant R01 CA166593) and Specialized Programs of Research Excellence (SPORE) (grant U54 CA 196519).

Address correspondence to: Lu Q. Le, Simmons Comprehensive Cancer Center, Hamon Center for Regenerative Science and Medicine, University of Texas Southwestern Medical Center, 5323 Harry Hines Boulevard, Dallas, Texas 75390-9069, USA. Phone: 214.648.5781; Email: lu.le@utsouthwestern.edu.

1. Monroe CL, Dahiya S, Gutmann DH. Dissecting clinical heterogeneity in neurofibromatosis type 1. *Annu Rev Pathol*. 2017;12:53–74.
2. Korf BR, Rubenstein AE. *Neurofibromatosis: a handbook for patients, families, and healthcare prfessionals*. 2nd ed. New York, New York, USA: Thieme; 2005.
3. Friedman JM, Gutmann DH, MacCollin M, Riccardi VM, eds. *Neurofibromatosis: phenotype, natural history, and pathogenesis*. 3rd ed. Baltimore, Maryland, USA: Johns Hopkins University Press; 1999.
4. Gutmann DH, Ferner RE, Listernick RH, Korf BR, Wolters PL, Johnson KJ. Neurofibromatosis type 1. *Nat Rev Dis Primers*. 2017;3:17004.
5. Ratner N, Miller SJ. A RASopathy gene commonly mutated in cancer: the neurofibromatosis type 1 tumour suppressor. *Nat Rev Cancer*. 2015;15(5):290–301.
6. Staser K, Yang FC, Clapp DW. Pathogenesis of plexiform neurofibroma: tumor-stromal/hematopoietic interactions in tumor progression. *Annu Rev Pathol*. 2012;7:469–495.
7. Riccardi VM. Von Recklinghausen neurofibromatosis. *N Engl J Med*. 1981;305(27):1617–1627.
8. Ferner RE. Neurofibromatosis 1. *Eur J Hum Genet*. 2007;15(2):131–138.
9. Jessen WJ, et al. MEK inhibition exhibits efficacy in human and mouse neurofibromatosis tumors. *J Clin Invest*. 2013;123(1):340–347.
10. Dombi E, et al. Activity of selumetinib in neurofibromatosis type 1-related plexiform neurofibromas. *N Engl J Med*. 2016;375(26):2550–2560.
11. Yoshida Y, Adachi K, Yamamoto O. Local mast cell histamine and plasma histamine levels in neurofibromatosis type 1. *Acta Derm Venereol*. 2010;90(6):637–639.
12. Brasfield RD, Das Gupta TK. Von Recklinghausen's disease: a clinicopathological study. *Ann Surg*. 1972;175(1):86–104.
13. Kamide R, Nomura N, Niimura M. Characterization of mast cells residing in cutaneous neurofibromas. *Dermatologica*. 1989;179 Suppl 1:124.

14. Isaacson P. Mast cells in benign nerve sheath tumours. *J Pathol*. 1976;119(4):193–196.
15. Geller M, Ribeiro MG, Araújo AP, de Oliveira LJ, Nunes FP. Serum IgE levels in neurofibromatosis 1. *Int J Immunogenet*. 2006;33(2):111–115.
16. Yang FC, et al. Nf1-dependent tumors require a microenvironment containing Nf1$^{+/-}$- and c-kit-dependent bone marrow. *Cell*. 2008;135(3):437–448.
17. Demestre M, et al. Imatinib mesylate (Glivec) inhibits Schwann cell viability and reduces the size of human plexiform neurofibroma in a xenograft model. *J Neurooncol*. 2010;98(1):11–19.
18. Riccardi VM. Mast-cell stabilization to decrease neurofibroma growth. Preliminary experience with ketotifen. *Arch Dermatol*. 1987;123(8):1011–1016.
19. Riccardi VM. A controlled multiphase trial of ketotifen to minimize neurofibroma-associated pain and itching. *Arch Dermatol*. 1993;129(5):577–581.
20. Riccardi VM. Ketotifen suppression of NF1 neurofibroma growth over 30 years. *Am J Med Genet A*. 2015;167(7):1570–1577.
21. Lennartsson J, Rönnstrand L. Stem cell factor receptor/c-Kit: from basic science to clinical implications. *Physiol Rev*. 2012;92(4):1619–1649.
22. Ding L, Saunders TL, Enikolopov G, Morrison SJ. Endothelial and perivascular cells maintain haematopoietic stem cells. *Nature*. 2012;481(7382):457–462.
23. Liao CP, Booker RC, Morrison SJ, Le LQ. Identification of hair shaft progenitors that create a niche for hair pigmentation. *Genes Dev*. 2017;31(8):744–756.
24. Richardson BE, Lehmann R. Mechanisms guiding primordial germ cell migration: strategies from different organisms. *Nat Rev Mol Cell Biol*. 2010;11(1):37–49.
25. Wernersson S, Pejler G. Mast cell secretory granules: armed for battle. *Nat Rev Immunol*. 2014;14(7):478–494.
26. Chen S, et al. Nf1$^{-/-}$ Schwann cell-conditioned medium modulates mast cell degranulation by c-Kit-mediated hyperactivation of phosphatidylinositol 3-kinase. *Am J Pathol*. 2010;177(6):3125–3132.
27. Ito T, et al. Stem cell factor programs the mast cell activation phenotype. *J Immunol*. 2012;188(11):5428–5437.
28. Yang FC, et al. Neurofibromin-deficient Schwann cells secrete a potent migratory stimulus for Nf1$^{+/-}$ mast cells. *J Clin Invest*. 2003;112(12):1851–1861.
29. Staser K, Yang FC, Clapp DW. Mast cells and the neurofibroma microenvironment. *Blood*. 2010;116(2):157–164.
30. Ingram DA, et al. Genetic and biochemical evidence that haploinsufficiency of the Nf1 tumor suppressor gene modulates melanocyte and mast cell fates in vivo. *J Exp Med*. 2000;191(1):181–188.
31. Zhu Y, Ghosh P, Charnay P, Burns DK, Parada LF. Neurofibromas in NF1: Schwann cell origin and role of tumor environment. *Science*. 2002;296(5569):920–922.
32. Wu J, et al. Plexiform and dermal neurofibromas and pigmentation are caused by Nf1 loss in desert hedgehog-expressing cells. *Cancer Cell*. 2008;13(2):105–116.
33. Zheng H, et al. Induction of abnormal proliferation by nonmyelinating schwann cells triggers neurofibroma formation. *Cancer Cell*. 2008;13(2):117–128.
34. Le LQ, Liu C, Shipman T, Chen Z, Suter U, Parada LF. Susceptible stages in Schwann cells for NF1-associated plexiform neurofibroma development. *Cancer Res*. 2011;71(13):4686–4695.
35. Jessen KR, Mirsky R. The origin and development of glial cells in peripheral nerves. *Nat Rev Neurosci*. 2005;6(9):671–682.
36. Chen Z, Liu C, Patel AJ, Liao CP, Wang Y, Le LQ. Cells of origin in the embryonic nerve roots for NF1-associated plexiform neurofibroma. *Cancer Cell*. 2014;26(5):695–706.
37. Toonen JA, Solga AC, Ma Y, Gutmann DH. Estrogen activation of microglia underlies the sexually dimorphic differences in Nf1 optic glioma-induced retinal pathology. *J Exp Med*. 2017;214(1):17–25.
38. Diggs-Andrews KA, Brown JA, Gianino SM, Rubin JB, Wozniak DF, Gutmann DH. Sex is a major determinant of neuronal dysfunction in neurofibromatosis type 1. *Ann Neurol*. 2014;75(2):309–316.
39. Robertson KA, et al. Imatinib mesylate for plexiform neurofibromas in patients with neurofibromatosis type 1: a phase 2 trial. *Lancet Oncol*. 2012;13(12):1218–1224.
40. Prada CE, et al. Neurofibroma-associated macrophages play roles in tumor growth and response to pharmacological inhibition. *Acta Neuropathol*. 2013;125(1):159–168.
41. Choi K, et al. An inflammatory gene signature distinguishes neurofibroma Schwann cells and macrophages from cells in the normal peripheral nervous system. *Sci Rep*. 2017;7:43315.
42. Sica A, Mantovani A. Macrophage plasticity and polarization: in vivo veritas. *J Clin Invest*. 2012;122(3):787–795.
43. Le LQ, Shipman T, Burns DK, Parada LF. Cell of origin and microenvironment contribution for NF1-associated dermal neurofibromas. *Cell Stem Cell*. 2009;4(5):453–463.
44. Ribeiro S, et al. Injury signals cooperate with Nf1 loss to relieve the tumor-suppressive environment of adult peripheral nerve. *Cell Rep*. 2013;5(1):126–136.
45. Rizvi TA, et al. A novel cytokine pathway suppresses glial cell melanogenesis after injury to adult nerve. *J Neurosci*. 2002;22(22):9831–9840.
46. Wise JB, Cryer JE, Belasco JB, Jacobs I, Elden L. Management of head and neck plexiform neurofibromas in pediatric patients with neurofibromatosis type 1. *Arch Otolaryngol Head Neck Surg*. 2005;131(8):712–718.
47. Nguyen R, Ibrahim C, Friedrich RE, Westphal M, Schuhmann M, Mautner VF. Growth behavior of plexiform neurofibromas after surgery. *Genet Med*. 2013;15(9):691–697.
48. Grivennikov SI, Greten FR, Karin M. Immunity, inflammation, and cancer. *Cell*. 2010;140(6):883–899.
49. Coussens LM, Werb Z. Inflammation and cancer. *Nature*. 2002;420(6917):860–867.
50. Anoush M, Mohammad Khani MR. Evaluating the anti-nociceptive and anti-inflammatory effects of ketotifen and fexofenadine in rats. *Adv Pharm Bull*. 2015;5(2):217–222.
51. Zhu Y, et al. Ablation of NF1 function in neurons induces abnormal development of cerebral cortex and reactive gliosis in the brain. *Genes Dev*. 2001;15(7):859–876.
52. Brannan CI, et al. Targeted disruption of the neurofibromatosis type-1 gene leads to developmental abnormalities in heart and various neural crest-derived tissues. *Genes Dev*. 1994;8(9):1019–1029.
53. Leone DP, et al. Tamoxifen-inducible glia-specific Cre mice for somatic mutagenesis in oligodendrocytes and Schwann cells. *Mol Cell Neurosci*. 2003;22(4):430–440.
54. Soriano P. Generalized lacZ expression with the ROSA26 Cre reporter strain. *Nat Genet*. 1999;21(1):70–71.
55. Biernaskie JA, McKenzie IA, Toma JG, Miller FD. Isolation of skin-derived precursors (SKPs) and differentiation and enrichment of their Schwann cell progeny. *Nat Protoc*. 2006;1(6):2803–2812.